Daniel Blum, Maren Reuter, Wolfgang Schliebs, Jana Tomaschewski, Ralf Erdmann* and Richard Wagner*

Membrane binding and pore forming insertion of PEX5 into horizontal lipid bilayer

https://doi.org/10.1515/hsz-2022-0183
Received May 16, 2022; accepted August 29, 2022;
published online October 20, 2022

Abstract: The assembly of the peroxisomal translocon involves the transition of a soluble form of the peroxisomal targeting receptor PEX5 into a membrane-bound form, which becomes an integral membrane component of the import pore for peroxisomal matrix proteins. How this transition occurs is still a mystery. We addressed this question using a artificial horizontal bilayer in combination with fluorescence time-correlated single photon counting (TCSPC) and electrophysiological channel recording. Purified human isoform PEX5L and truncated PEX5L(1–335) lacking the cargo binding domain were selectively labeled with thiol-reactive Atto-dyes. Diffusion coefficients of labeled protein in solution show that PEX5L is monomeric with a rather compact spherical conformation, while the truncated protein appeared in a more extended conformation. Labeled PEX5L and the truncated PEX5L(1–335) bind stably to horizontal bilayer thereby accumulating around 100-fold. The diffusion coefficients of the membrane-bound PEX5L forms are 3–4 times lower than in solution, indicating the formation of larger complexes. Electrophysiological single channel recording shows that membrane-bound labeled and non-labeled PEX5L, but not the truncated PEX5L(1–335), can form ion conducting membrane channels. The data suggest that PEX5L is the pore-forming component of the oligomeric peroxisomal translocon and that spontaneous PEX5L membrane surface binding might be an important step in its assembly.

Keywords: membrane binding; peroxisomes; peroxisomal protein import; PEX5; pore formation; protein import.

Introduction

Matrix protein import into peroxisomes shows fundamental differences to protein import into many other organelles as peroxisomes import folded and even oligomerized proteins in a largely unknown translocation mechanism. The peroxisomal import receptors alternate between a soluble form in the cytosol and a cargo-loaded form that associates with the peroxisomal membrane, thereby becoming part of a transient transition pore (Erdmann and Schliebs 2005; Meinecke et al. 2010). The PEX5-cargo complexes target a docking and translocation complex at the peroxisomal membrane, where PEX5 is subsequently inserted into the membrane, ATP-independently, as an essential part of the translocon complex. The membrane-associated PEX5L-is then monoubiquitinated at a C-terminal conserved cysteine residue and extracted from the membrane as a ubiquitin-PEX5 conjugate back into the cytosol in an ATP-dependent manner (Alencastre et al. 2009; Meinecke et al. 2016; Walter and Erdmann 2019). Recently, it has been reported that PEX5 is also transported into peroxisomes and exported back to the cytosol via the peroxisomal ubiquitin ligase complex.

The formation of the peroxisomal translocon for matrix proteins is a multistep process initiated by the binding of folded cargo proteins to cytosolic receptors. The human import receptor PEX5 recognizes proteins that carry a type 1 peroxisomal targeting signal (PTS1). There are two splice variants of PEX5. PEX5S (short) binds PTS1 proteins, while PEX5L (Long) binds PTS1 proteins but also PEX7, the receptor for PTS2 proteins (Rucktäschel et al. 2011; Walter and Erdmann 2019). These interactions are proposed to lead to conformational changes of the receptors, which in turn allow the receptor-cargo complexes to dock at the peroxisomal membrane. Together with the docking protein PEX14, both PEX5L and PEX5S are supposed to become integral components of peroxisomal protein import channels. The assembly of the translocons is

***Corresponding authors: Ralf Erdmann**, Institut für Biochemie und Pathobiochemie, Abt. Systembiochemie, Medizinische Fakultät, Ruhr-Universität Bochum, D-44801 Bochum, Germany,
E-mail: ralf.erdmann@rub.de; and **Richard Wagner**, MOLIFE Research Center, Jacobs, University Bremen, D-28759 Bremen, Germany,
E-mail: ri.wagner@jacobs-university.de. https://orcid.org/0000-0001-5472-8097 (R. Wagner)
Daniel Blum, MOLIFE Research Center, Jacobs, University Bremen, D-28759 Bremen, Germany
Maren Reuter, Wolfgang Schliebs and Jana Tomaschewski, Institut für Biochemie und Pathobiochemie, Abt. Systembiochemie, Medizinische Fakultät, Ruhr-Universität Bochum, D-44801 Bochum, Germany

thought to occur mainly through interactions of the receptors with peroxisomal phospholipids and PEX14, either simultaneously or sequentially (Meinecke et al. 2016; Walter and Erdmann 2019). It is not yet known how the soluble form of PEX5/PEX5-cargo complexes is converted into a membrane-bound form and how the receptor does become an integral component of the import pore (Meinecke et al. 2016; Walter and Erdmann 2019). The yeast translocon has been shown to consist predominantly of PEX5 and PEX14 (Meinecke et al. 2010). In an accompanying paper in this special issue, it is shown that this also accounts for the human PEX5-complex, which also shows pore activity (Ghosh et al. 2022). How its major constituents, PEX5 and PEX14, contribute to pore formation is not known.

We analyzed the oligomeric state of PEX5 in solution and the binding of soluble PEX5 to artificial horizontal bilayer membranes using the scanning fluorescence time-correlated single photon counting (TCSPC) technique (Becker et al. 2006; Felekyan et al. 2005; Jameson et al. 2009). In addition, using the combined opto-electrical horizontal lipid bilayer (HLB) technique (Bartsch et al. 2012; Honigmann et al. 2012; Wagner et al. 2018), we tested whether the membrane-bound receptor PEX5 alone affects the electrical membrane permeability by pore-forming activity. Our results show that (i) purified PEX5L in solution resides mainly in the monomeric state, (ii) PEX5L enriches at the bilayer membrane surface and becomes stably bound at/in the membrane, (iii) after membrane binding PEX5L but not the truncated PEX5(1–335) induces voltage-driven ionic currents with ion-channel characteristics within our artificial lipid bilayer systems. Our data suggest that PEX5L is the pore-forming component of the oligomeric peroxisomal translocon.

Results

Hydrodynamic properties of PEX5 in solution-lateral and rotational diffusion of PEX5 in solution

Purification and labeling of recombinant human PEX5L

For the fluorescence spectroscopic investigations, it was necessary to covalently label PEX5L selectively with suitable fluorescent dyes. For this purpose, NEM derivatives of Atto dyes (Atto TEC GmbH, 57074 Siegen, Germany) were used for covalent binding to PEX5 cysteines. PEX5L (uniprotKB accession P50542) contains six cysteines (Figure 1A). The five cysteines located in the C-terminal tetratricopeptide repeats (TPR) domain are not accessible in the folded state, while Cys11 in the disordered *N*-terminal region (amino acids 1–335) is easily accessible for chemical modification. Figure 1B shows the Coomassie-stained SDS-Gel of the purified PEX5L and the truncated PEX5L (1–335). Additional polypeptides were identified by immunoblot analyses as derivatives of the PEX5 forms, either degradation products or oligomers.

Labeling of the different PEX5L samples was performed as described in detail in Materials and Methods. The degree of labeling (DOL) with the different NEM-reactive Atto-dyes was determined spectroscopically (see Materials and

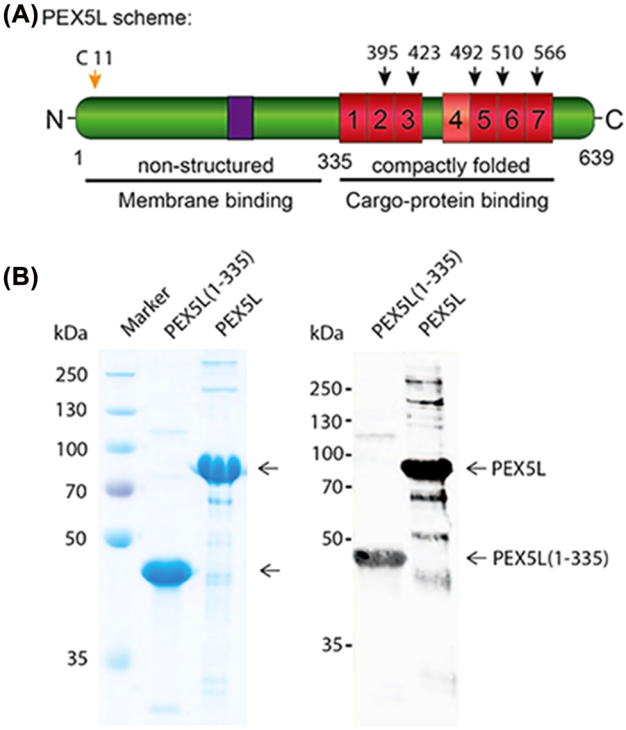

Figure 1: Purification of proteins used for Atto labeling. The long isoform of human recombinant PEX5, PEX5L, and an *N*-terminal fragment, PEX5L(1–335) were used for cysteine-labeling.
(A) The scheme represents the position of cysteines in the represented polypeptide sequence of human PEX5L (marked by arrows). PEX5L consists of 635 amino acids, including the exon-coded PEX7 binding domain (purple). The *N*-terminal disordered fragment PEX5L(1–335) contains only one cysteine at position 11, which is supposed to be accessible for labeling. The five remaining cysteines in the *C*-terminal cargo-binding domain are buried within the globular alpha-helical structure formed by the seven TPR-domains (red boxes). (B) His6-tagged PEX5L and PEX5L(1–335) were expressed in *E. coli* and affinity-purified on a Ni-NTA column and further by ion exchange chromatography. Eluate fractions (protein concentration 10 mg/ml) were analyzed by SDS-PAGE and Coomassie staining (left panel) or immunoblotting using polyclonal anti PEX5 antibodies (right panel).

Methods for details). A representative example of the obtained degree of PEX5L labeling with the NEM-reactive fluorescence dyes is shown in Table 1. The results suggest that only one cysteine is labeled, presumably the *N*-terminal one, which is fully accessible (Figure 1A).

Diffusion of fluorescence-labeled PEX5L in solution indicates that the soluble PTS1 receptor resides mainly in the monomeric state

The basic outline of the (TCSPC) technique and the methods for analyzing TCSPC data in combination with the microscopic artificial horizontal bilayer technique (HLB) are shown schematically in Figure 6 (Materials and Methods) and described in detail elsewhere (Bartsch et al. 2012, 2013a; Honigmann et al. 2012). We applied the TCSPC technique in combination with the HLB technique (Bartsch et al. 2012) and investigated the diffusion of the NEM-Atto647N labeled PEX5L in solution and after binding to the horizontal bilayer membrane.

The FCS and FIDA analysis of TCPSC recordings of PEX5L-Atto647N revealed identical results with respect to the fraction of the PEX5L-bound dye, indicating that the label does not interfere with diffusion properties. Two different components were observed with respect to fluorescence intensity (molecular brightness [q]) as well as with regards to the diffusion time (Figure 2A and B). The smaller relative fractions ($f_{rel} \cong 0.2$) were comparable in both analyzed features. We propose that the faster diffusion component has to be attributed to the diffusion of remaining free Atto647N dye in the sample since τ_{diff} (fast) is almost of the same magnitude as τ_{diff} = 55 µs of the free Atto655 used for the calibration of the confocal volume (data not shown, [Müller et al. 2008]). Interestingly, the molecular brightness of the less frequent component ($f_{rel} \cong 0.2$) was significantly lower than the more frequent component ($f_{rel} \cong 0.8$), indicating that binding of the dye to the protein appears to be accompanied by a drastic increase of the brightness of Atto647N. Next, we analyzed the rotational diffusion of labeled PEX5L in solution using the fluorescence lifetime-anisotropy (Smith and Ghiggino 2015).

Table 1: Degree of PEX5L labeling with the NEM-reactive fluorescence dyes.

DOL (degree of labeling)	
Sample	**DOL**
PEX5L (1–335)-Atto647N	0.8 ± 0.1 (n = 5)
PEX5L-Atto647N	1.01 ± 0.15 (n = 5)

The fluorescence polarization anisotropy measurements (Figure 3A) revealed three decay components, two fast ones (τ_1 = 0.8 ns, τ_2 = 1.06 ns) and a third one with minor amplitude ($f_a \cong 0.3$) and $\tau_{rot} \cong 28$ ns. This decay component presumably can be attributed to the rotation of PEX5L (Figure 3B). The FCS and the fluorescence anisotropy measurements resulted in a lateral diffusion coefficient of $D_{\mathrm{lat}} = 65\,\mu^2 \cdot \mathrm{s}^{-1}, \tau_{\mathrm{lat}} = 300\,\mu\mathrm{s}$ and a rotational diffusion coefficient of $D_{\mathrm{rot}} \approx 3.6 \cdot 10^7\,\mathrm{s}^{-1}$, ($\tau_{rot} \approx 28$ ns) for the fluorescent labeled PEX5L (Figures 2A and 3A). Using hydrodynamic calculations, conclusions about the oligomeric state of PEX5L in solution can be drawn from these diffusion times. Details of this hydrodynamics calculations are given in the Materials and Methods section and summarized in Figure 3B, C. Figure 3B shows the calculated τ_{lat} as a function of the oligomeric state, whereby the *x*-scale index N_i represents the number (i) of spherical PEX5L units in the oligomer. Correspondingly, Figure 3C shows the calculated τ_{rot} as the function of the oligomeric state. For details of the calculations see also Materials and Methods section. As obvious from Figure 3B and C, the calculated translation diffusion coefficient and the corresponding τ_{lat} = 302 µs as well as the calculated rotational diffusion coefficients with corresponding τ_{rot} = 23 ns for PEX5L Atto647N in solution are compatible with monomeric PEX5. Moreover, for PEX5L Atto647N, the diffusion times (τ_{lat} and τ_{rot}) were within an error limit of ±4.5% identical to the one given in Table 2.

Soluble PEX5L accumulates on the membrane in the HLB system

Using the microscopic HLB-technique, we investigated binding of the labeled PEX5L and the labeled *N*-terminal deletion mutant PEX5L(1–335) to a horizontal lipid bilayer. After addition of 12 nM PEX5L-Atto647-to the cis compartment, time series of *x*–*z* scans in the HLB with a *z*-stepping of 250 nm were performed. Figure 4A and B show representative examples of the measurements.

The diffusion time of PEX5LAtto655 in the cis compartment with confocal volumes located in the cis compartment above the bilayer was τ_{lat} = 300 ± 40 µs (n > 12). To determine the diffusion time of the labeled PEX5L at the membrane, we used diffusion time data obtained at multiple *Z*-positions to determine the principal one at the bilayer (see Materials and Methods). We thus determined the maximal τ_{lat} value in the 250 nm *z*-stepping scans along the *z*-axis (see Materials and Methods), and obtained a value of τ_{lat} (mem) = 1.5 ± 0.08 ms (n = 5). The diffusion time in the cis compartment compares

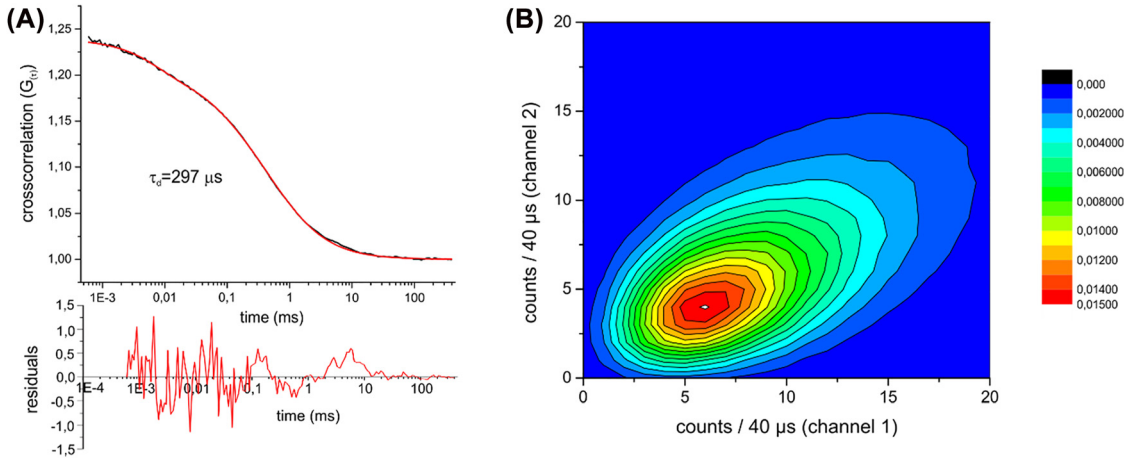

Figure 2: FCS (A) and FIDA (B) analysis of TCPSC recordings of PEX5L-Atto647N in standard buffer (see materials and methods for details).

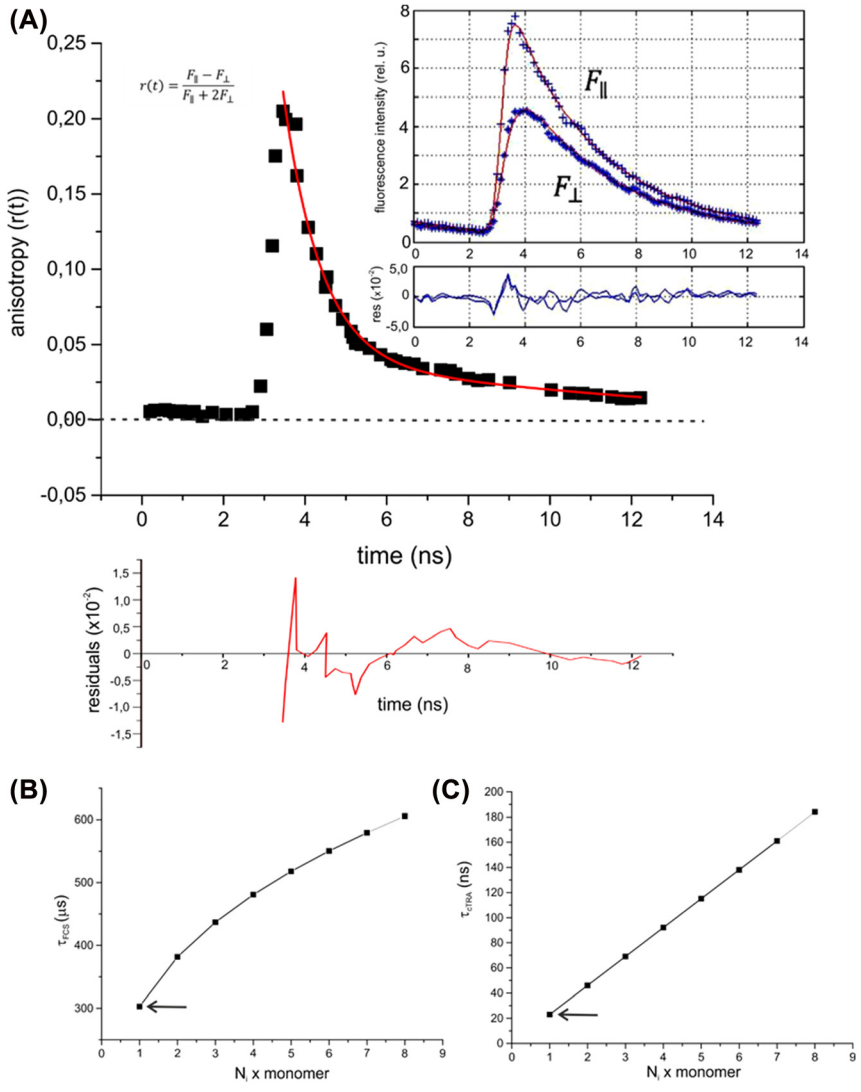

Figure 3: Rotational diffusion of Pex5 in solution.
(A) Fluorescence polarization anisotropy ($r(t)$) obtained from the polarized fluorescence lifetime (inset) of PEX5L-Atto647N in solution. (B) Calculated lateral diffusion coefficient (τ_{lat}) for PEX5L as a function of its oligomeric state (see Materials and Methods for details).
(C) Calculated rotational diffusion coefficient (τ_{rot}) for PEX5L as a function of its oligomeric state (see Materials and Methods for details).

Table 2: FCS and FIDA analysis of TCPSC recordings of labeled PEX5L-Atto647N.

FCS			FIDA	
Diffusion time (μs)[a]	**Diffusion coefficient (μm·s^{-1})[a]**	**Fraction[a]**	**Molecular brightness (q/kHz)[a]**	**Fraction[a]**
50 ± 10	410	0.2 ± 0.02 (n = 5)	33 ± 5	0.21 ± 0.025 (n = 3)
297 ± 22	65	0.8 ± 0.015 (n = 5)	110 ± 12	0.79 ± 0.031 (n = 3)

[a]Confocal focus area = 0.31 μm^2.

Table 3: Diffusion coefficients of labeled PEX5L and truncated hsPEX5L(1–335).

	Diffusion coefficient (μm^2·s^{-1}) solution	**Diffusion coefficient (μm^2·s^{-1}) membrane**
PEX5L	65 ± 6.7 (n = 5)	16 ± 3.2 (n = 3)
PEX5L(1–335)	82 ± 5.7 (n = 5)	0.1 ± 0.02 (n = 3)

well with the one obtained for the labeled PEX5L in solution (Figure 2, Table 3), while τ_{lat} of the labeled PEX5L at the bilayer shows that the membrane-bound PEX5L became immobilized at the membrane (Table 3). It is important to note that the binding of the labeled PEX5L to the membrane was long-term stable and repeated z-scans during a period of 15 min gave repetitively constant τ_{lat} (mem) values. Next, we tested whether the truncated N-terminal PEX5L(1–335), which is presumed to be mainly in an extended, disordered conformation (Shiozawa et al. 2009) and important for the interaction of PEX5L with the membrane (Costa-Rodrigues et al. 2005), also binds to the membrane. Figure 4B and D shows z-scans of an HLB after addition of 12 nM Atto488--labeled PEX5L(1–335) to the cis compartment (upper part) and below a z-scan of the same bilayer after five perfusions of the cis compartment, while the right parts of Figure 4A shows the corresponding fluorescence intensity profiles along the z-axis. Figure 4D shows the FCS measurement of

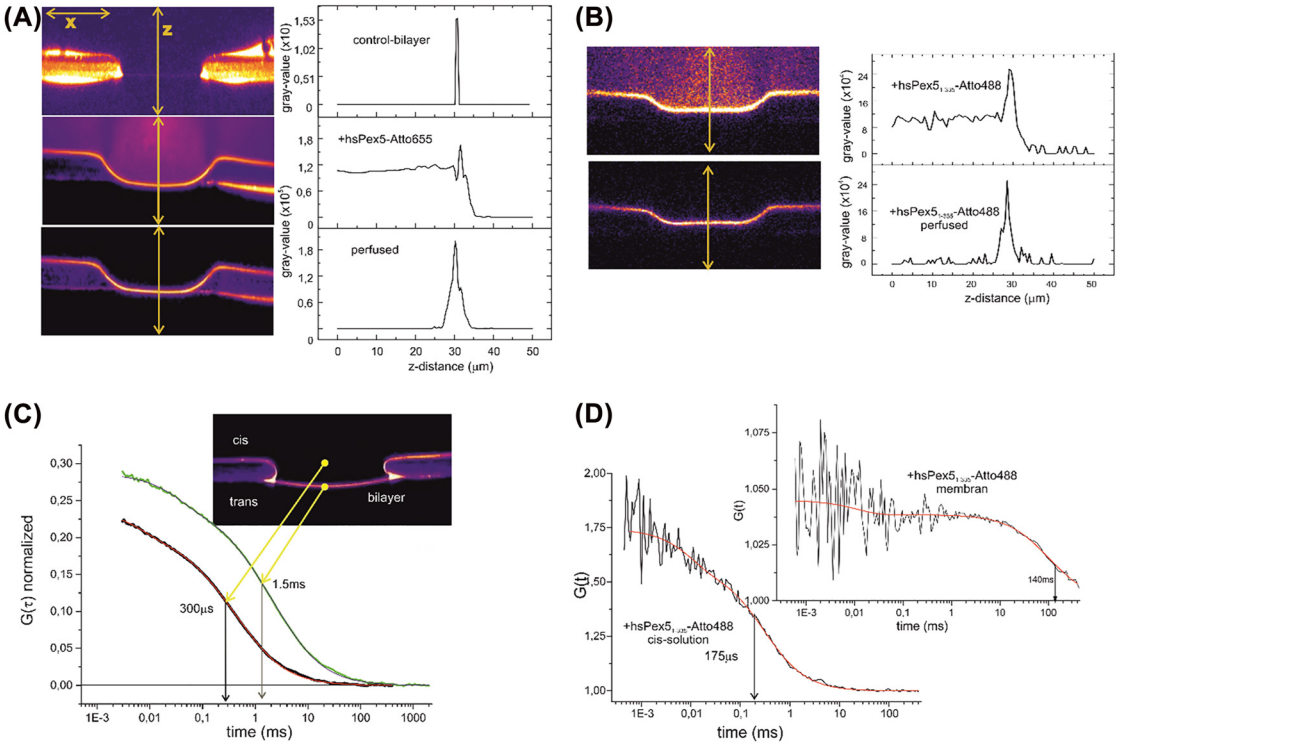

Figure 4: x–z scans from horizontal lipid bilayer (HLB) and HLB-FCS measurements of labeled PEX5L and the N-terminal PEX5L(1–335). (A) Top, empty-control bilayer, (middle) same bilayer, but after addition to 1 nM Atto655-labeled PEX5L (DOL = 1.08) to the cis compartment, (bottom) same HLB but after 5 times perfusion of the cis compartment. (B) Bilayer after addition to 1 nM Atto488-labeled PEX5L(1–335) (DOL = 0.97) to the cis compartment, (bottom) same HLB but after 5 times perfusion of the cis compartment. (C) Confocal FCS measurements from the same bilayer as in (A, bottom). The location of the confocal volumes is indicated. (D) Confocal FCS measurements from the same bilayer as in (B, bottom). The confocal volume along the z-coordinate was positioned in the bilayer (see [C]). The location of the confocal spot along the z-direction in the HLB-setup is indicated in Figure 4C (right part) and the corresponding FCS curves are shown in Figure 4C and D on the right.

the Atto488-labeled PEX5L(1–335) in the cis compartment and at the membrane. The diffusion coefficient in solution calculated from τ_{lat} = 175 µs was $D_{lat} \equiv 82 \pm 5.7 \frac{\mu m^2}{s}$. Considering the molecular mass of PEX5L(1–335) (Mr = 37.5 kDa), this value clearly indicates that the PEX5L(1–335) protein has a much lower density packed conformation, since a globular protein with this Mr would result in a diffusion time of $\tau_{lat} \cong 145$ µs (see Materials and Methods for the calculation). However, when membrane bound (Figure 4C), the diffusion time of Atto488 labeled PEX5L(1–335) slowed down drastically to τ_{lat} = 140 ms (Figure 4D). If the accumulation of the two proteins on the membrane is determined from an *x–z* scan, using the ratio of the area-related fluorescence intensity above the bilayer (cis-compartment) to the area-related fluorescence intensity in the bilayer, enrichment factors of *f* = 50–200 are determined.

In summary, our results with the HLB-technique show that the labeled PEX5L and the truncated *N*-terminal PEX5L(1–335) bind so tightly to the horizontal bilayer membrane that repeated perfusion of the cis compartment does not lead to detachment of the fluorescence-labeled proteins. Both PEX5 variants are strongly bound and became largely immobilized on the bilayer membrane. Remarkably, the truncated *N*-terminal PEX5L(1–335) was either nearly completely integrated in the membrane thus drastically slowing down the diffusion rates (see Table 3) and/or the truncated protein forms very large oligomers in the membrane.

Binding of PEX5L to the bilayer membrane induced ion channel activity

With HLB-system parallel and/or simultaneous optical and electrical recording from the bilayer are feasible (Bartsch et al. 2012). We performed high resolution electrical recordings from HLBs after addition of labeled and non-labeled PEX5L. In extremely rare cases (≤1%), voltage driven membrane ion currents with a wide range of current characteristics were observed.

Figure 5A shows current recordings from a bilayer in response to a voltage-gate (duration 10 s) with the indicated voltage amplitude. Figure 5B shows a current recording from the same bilayer in response to a voltage ramp. Bilayer currents were observed after addition of 1 µl (1 mg/mL) purified PEX5L into a volume of 1.2 mL of the cis compartment in a classical vertical bilayer setup, see Bartsch et al. (2013b) for a practical guideline for the lipid bilayer technique and references (Kramar et al. 2010; Miller 2013; Patlak 1993; Sakmann 2013) for the theory underlying the analysis of single channel properties. PEX5L has been produced by heterologous expression in a porin-deficient *Escherichia coli* mutant strain BL21(DE3)omp8 (Prilipov et al. 1998) with subsequent purification to an extent that no other polypeptides as Pex5 or PEX5 derivatives could be detected. No other polypeptides beside PEX5 or PEX5 derivatives were be detected (Figure 1B and Materials and Methods). It is important to note that in all the different MOK samples, neither with the classical vertical bilayer setup nor in the HLB-setup, no channel activity was observed. The expanded current trace at V_{cmd} = −60 mV (Figure 5C), the all point amplitude histogram at V_{cmd} = −60 mV (Figure 5D) and the mean variance plot at V_{cmd} = −60 mV (Figure 5E) allow a first analysis of the observed pore activity. The histogram (Figure 5D) reveals three open channel states at V_{cmd} = −60 mV, i_1 = −21 pA, i_2 = −44 pA and i_3 = −91 pA, while the mean variance plot shows that the main gating transition occurred between i_2 and i_3 with Δi_{main} = 47 pA and a second transition between i_1 and i_2 with Δi_{sub} = 24 pA. These values correspond to channel conductance states of G_{main} = 780 pS and G_{sub} = 390 pS. Both conductance states appeared independent of each other and no gating transitions with $\Delta G = G_{main} + G_{sub}$ was observed (see mean variance plot Figure 5E), indicating that at least two different membrane pores were formed. The current voltage relation from the same bilayer revealed in a voltage ramp (Figure 5B) a slight rectification with slope conductance of $G_{slope} \approx 380$ pS but only a negative V_{cmd}.

Figure 5F–H shows electrical current recordings from a HLB setup after addition of 12 nM Atto488-PEX5L to the cis compartment. Voltage gates with the indicated V_{cmd} were applied (Figure 5F) and the current-voltage relation (Figure 5G) was calculated from the mean currents in Figure 5F. The enrichment of the labeled protein on the bilayer surface is shown in Figure 4B. The slope conductance in the calculated i/V relation (Figure 5G) was identical to the one in the current voltage ramp (Figure 5H) from the same bilayer G_{slope} = 1.5 nS. While the unlabeled PEX5L displayed rather frequent gating activity with brief channel closures (Figure 5A, B and D), the Atto488-labeled PEX5L (Figure 5F–H) remained complete in the open state. The rather high slope conductance may indicate that several open channels were present in the bilayer (Figure 5F–H).

The single channel recordings shown in Figure 5 are not representative of the pore activities observed after reconstitution of PEX5L or Atto labeled PEX5L in the classic vertical bilayer or the HLB setup, rather they represent examples of the endpoints of a wide range of observed pore activities: voltage induced current recordings with clearly structured gating events and clearly assignable

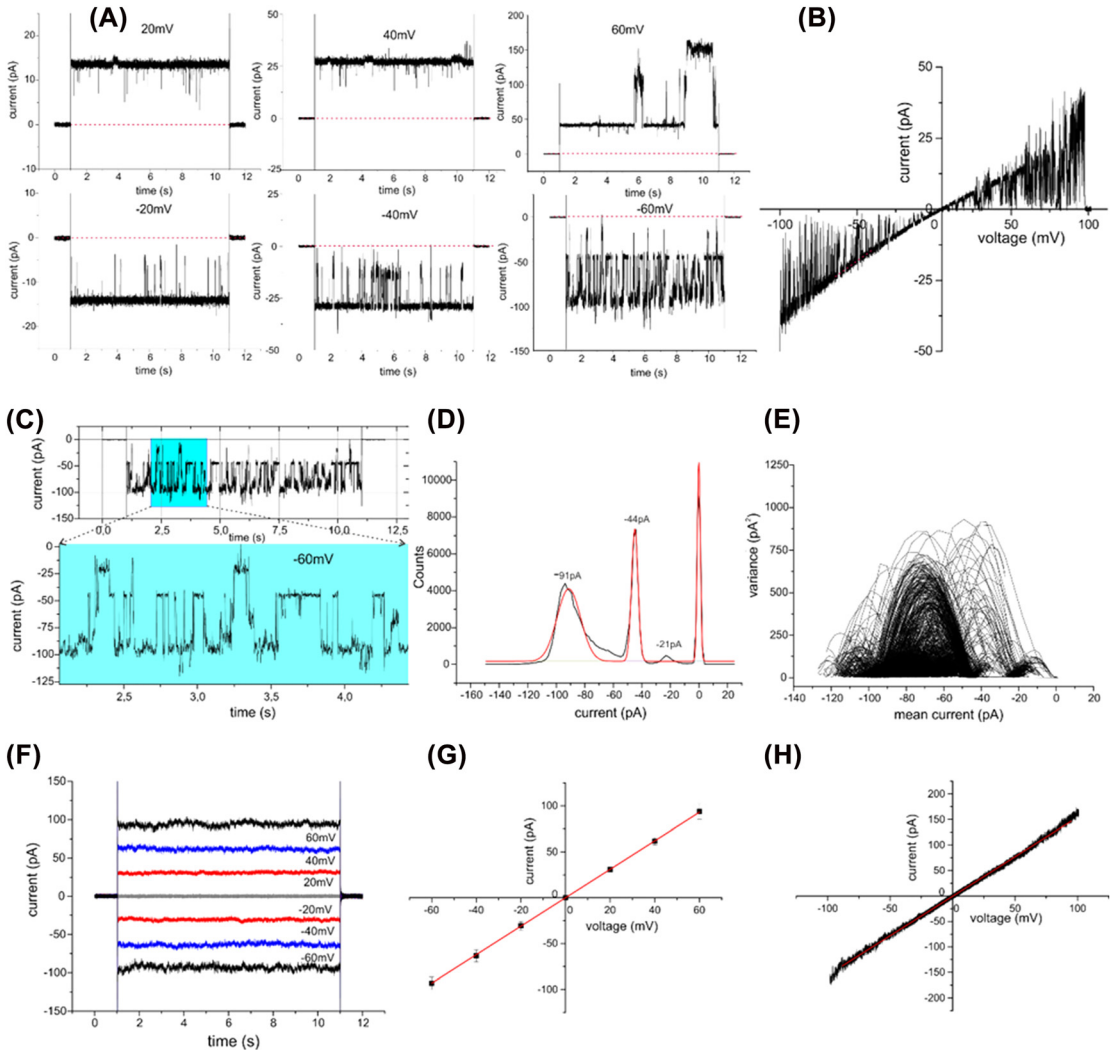

Figure 5: Electrical recordings from bilayer experiments after addition of PEX5L to the cis compartment of a vertical bilayer setup (A–E) and addition of PEX5L-Atto488 (DOL = 1) to the cis compartment of an HLB-setup.
(A) Single channel recording after integration of PEX5L in a vertical bilayer setup, with the given voltage gates. (B) Current-voltage ramp ($V_{cmd} \pm 100$ mV). (C) Expansion plot of the recording with $V_{cmd} = -60$mV. (D) All point amplitude histogram of the recording with $V_{cmd} = 60$ mV. (E) Mean variance plot of the recording (C) with $V_{cmd} = -60$ mV. (F) Current recordings after reconstitution of PEX5L-Atto488 in response to voltage gates with the indicated V_{cmd}-amplitudes. (G) Calculated current voltage relation from the records in (F). (H) Current voltage ramp from the same bilayer (F).

conductances on the one hand – and on the other – current recordings that only show a sometimes large conductance with clearly linear current-voltage characteristics across the membrane. Even if it is not yet entirely clear how PEX5 is integrated into the membrane in detail, it seems remarkable that PEX5L is integrated into the membrane in such a way that ion-conducting pores are formed, albeit with very heterogenous properties. Finally, important to note is that the truncated PEX5L(1–335) did not show any ion channel activity, although the protein seems to be even more deeply embedded in the membrane as shown by the very slow diffusion rate in/at the membrane.

Discussion

In the present work, we investigated the binding of soluble PEX5L and the truncated *N*-terminal PEX5L(1–335) to artificial lipid membranes using the high-resolution TPSC fluorescence techniques and electrical single channel recording. A major aim was to examine the extent to which the binding of fluorescence-labeled and unlabeled PEX5L to the membrane affects the electrical properties of the membrane. In all known models for the import of matrix proteins into the peroxisomes, PEX5 plays a central role as a cycling receptor. PEX5 shuttles from a cytosolic state to a

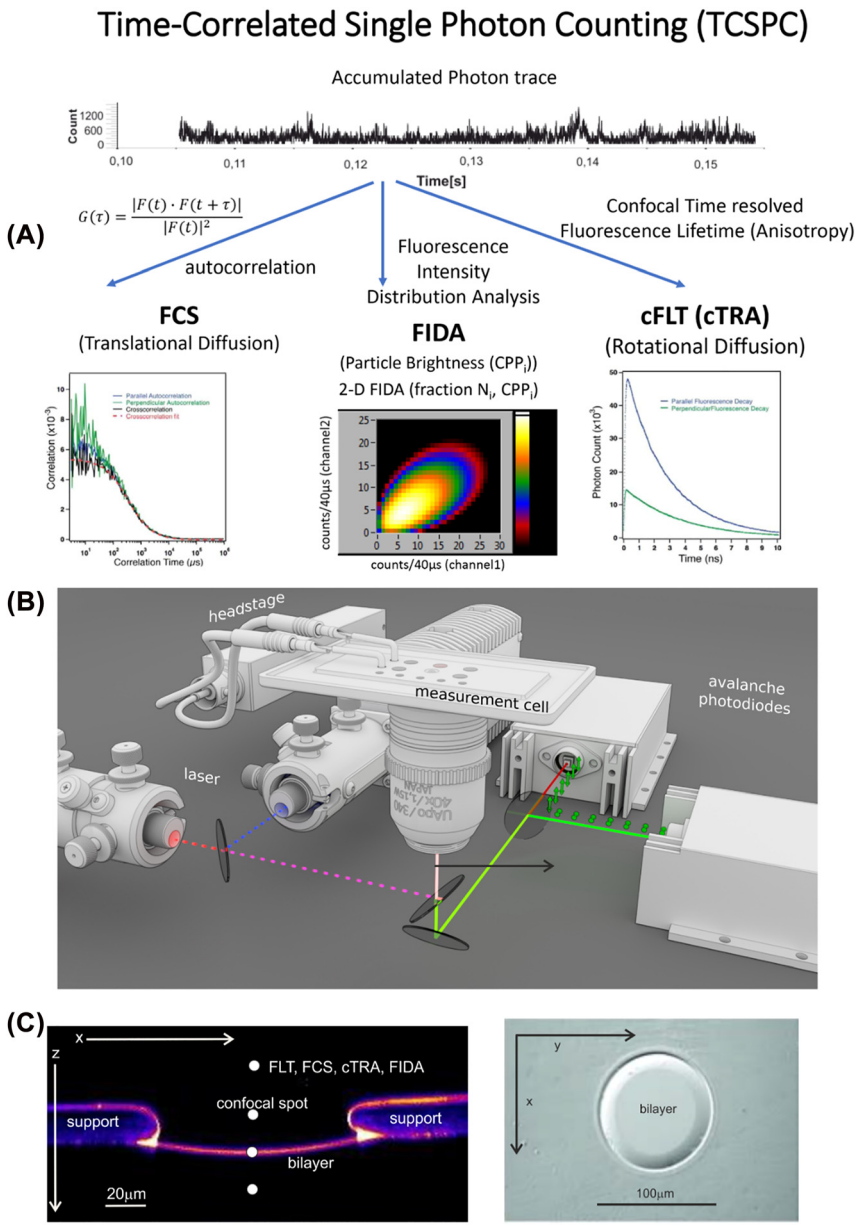

Figure 6: Principle features of scanning time correlated single photon counting (TCSPC) technique delivering fluorescence correlation (FCS) or cross correlation (FCCS), fluorescence intensity distribution and fluorescence lifetime and fluorescence anisotropy data simultaneously. (A) Schematic overview of the principal setup and experimental procedures for the recording of time-correlated-single photon events (top) and their analysis using fluorescence correlation spectroscopy (FCS) (left), analysis of fluorescence intensity distribution (FIDA) (middle) and confocal-time-resolved-fluorescence-lifetime-anisotropy (cFLT, cTRA) (right). (B) Experimental setup of the -confocal-scanning-single-photon-counting spectrometer with simultaneous single-channel electrophysiological recording. (C) *X–Z* scan of a fluorescent doted free-standing horizontal bilayer with 50 nm *z*-stepping images (left) and *X–Y* scan with 200 nm *Y*-stepping images(right).

central membrane component of the peroxisomal translocon and back to the cytosol. The assembly of the peroxisomal translocon involves the transition of a soluble form of the peroxisomal targeting receptor PEX5 into a membrane-bound form, which becomes an integral membrane component of the import pore for peroxisomal matrix proteins. How this transition occurs is still a mystery. Regarding this chimeric property of PEX5 as being water soluble in the cytosol and a membrane protein as part of the peroxisomal translocon, there are significant analogies to pore-forming toxins (PFTs). These PFTs also undergo metamorphosis from water soluble inactive monomers to transmembrane oligomeric complexes (Dal Peraro and Van Der Goot 2016). Our data suggest a primarily monomeric state of PEX5 in solution. This is in accordance with previous studies on the solution structure of PEX5L, PEX5L-cargo and PEX5L-Cargo-PEX14 complexes, demonstrating that PEX5 in solution is a monomer with an extended, coiled *N*-terminal part (Costa-Rodrigues et al. 2005; Shiozawa et al. 2009). So far only a few binding studies of PEX5 to model membranes have been reported. Within the *Saccharomyces cerevisiae* Pex5p sequence, regions have been identified that interconnect the receptor-cargo complex with the docking complex (Kerssen et al. 2006). In the same study, spontaneous association of the recombinant yeast and human PTS1 receptors with liposomes could also be demonstrated. The membrane interactions of the PEX5 *N*-terminal intrinsically disordered domain (NTD) and PEX14 NTD have been further supported *in vitro* by membrane mimicking bicelles and nanodiscs (Gaussmann et al. 2021). A recent study reports that PEX5 recycling is initiated by an

amphipathic helix in the *N*-domain that binds to the luminal side of the ubiquitin ligase (Skowyra and Rapoport 2022). Our results support previous studies of membrane-binding of PEX5 and further add that in an equilibrium situation PEX5 accumulates at the membrane. While the diffusion coefficient of PEX5 in the solution above the membrane show its free diffusion in a monomeric state, the diffusion of the protein at the membrane is drastically slowed down, indicating that the protein is largely immobilized. Interestingly the truncated PEX5L(1–335) showed even stronger interaction with the membrane with nearly complete immobilization. After association of both proteins, PEX5L and truncated PEX5L(1–335) with the membrane, they remained stably bound at the membrane. Even upon removal of excess of the protein that was in contact with the membrane surface by perfusion both proteins remained stably bound to the membrane. The increase in the concentration of PEX5L at the membrane interface could play an important role during the formation of the functional translocon oligomer.

Single channel recordings with membrane bound PEX5L and Atto488-conjugated PEX5L in the classical vertical bilayer as well as in the HLB setup allowed investigation of pore forming activity of both membrane-bound proteins. We observed pore forming activity of both full-length proteins. However, the truncated PEX5L(1–335) did not show any ion channel activity, indicating that the C-terminal cargo-binding domain is important for pore organization. Our data support the notion that PEX5 is the pore-forming component of the peroxisomal translocon. This has also been suggested by a study in yeast reporting that under certain circumstances PEX14 is dispensable for peroxisomal protein import. Upon overexpression of PEX5, the receptor can bind to the peroxisomal membrane and promote import of certain PTS1 proteins in the absence of PEX14 (Salomons et al. 2000). The observed ion conducting membrane pores formed by PEX5L displayed a large variety of conductance properties. At the present stage this variety does not allow to ascribe this activity to a particular membrane pore and requires further systematic investigation. It should be noted that affinity-purified PEX5 complexes from yeast and human cells (Ghosh et al. 2022; Meinecke et al. 2010) that many consist of PEX5 and PEX14 constitute large dynamic pores in the vertical bilayer system. Therefore, it seems plausible that Pex5-associated proteins at the peroxisomal membrane, i.e. he docking proteins Pex14 and Pex13 fulfill critical functions for proper assembly of the peroxisomal import pore. However, our data suggest that PEX5L is the pore-forming component of the oligomeric human peroxisomal translocon and that spontaneous PEX5L membrane surface binding might be an important step in its assembly.

Materials and methods

Heterologous expression and purification of PEX5 variants

E. coli expression plasmids encoding His6-tagged human PEX5L and PEX5L(1–335) were described previously (Schliebs et al. 1999). Expression and purification of the His6-tagged PEX5 variants was performed using Ni-NTA-agarose (Co) prepared in empty Chromabond columns for solid-phase extraction (Macherey-Nagel) followed by ResourceQ ion exchange column (GE Healthcare) chromatography using an Äkta purifier HPLC system according to the manufacturer's instructions (GE Healthcare). *E. coli* lysates were prepared by EmulsiFlex-C5 High Pressure homogenizer (Avestin) in presence of protease inhibitor mix containing 8 mM Antipain, 0.3 mM Aprotinin, 1 mM Benzamidin hydrochloride, 1 mM Bestatin, 10 mM Chymostatin, 5 mM Leupeptin, 5 mM sodium fluoride, 15 mM Pepstatin A and 1 mM phenymethylsulfonylfluoride. The lysate and all washing and elution buffers at pH 8.0 were supplemented with 1 mM dithiothreitol.

Labeling of PEX5

Chemical modification of both PEX5 variants was performed essentially according to the manufacturer's instructions (Atto TEC GmbH, Product Information: Thiol-Reactive Atto-Label (Maleimides). Standard procedure in brief: 1–2 mg/mL PEX5 in PBS buffer (Phosphate-Buffered Saline, pH 7.2) was incubated with the reactive fluorophore $\left(\frac{c_{\mathrm{dye}}\,(M)}{c_{\mathrm{protein}}\,(M)} = 1.5\right)$ for 2 h at room temperature. The labeled protein and the unbound dye were separated by size-exclusion chromatography using either a NAP™ 5 (GE Healthcare) column or a Superdex 200 10/300 GL (GE Healthcare) HPLC column. The degree of labeling (DOL) of both NEM-Atto647, NEM-Atto665, NEM-Atto488, NEM-labeled proteins PEX5L was determined using the following relations: $\mathrm{DOL} = \frac{c(\mathrm{dye})}{c(\mathrm{protein})} = \frac{A_{\mathrm{max}}/\epsilon_{\mathrm{max}}}{A_{\mathrm{protein}}/\epsilon_{\mathrm{protein}}} = \frac{A_{\mathrm{max}}\cdot\epsilon_{\mathrm{protein}}}{(A_{\mathrm{max}} - A_{\mathrm{max}}\cdot CF_{280})\cdot\epsilon_{\mathrm{max}}}$.

In order to optimize the wavelength dependent confocal-volume different ATTO dyes (Atto488, Atto647N, Atto655) were used. The diffusion-times for the differently labeled PEX5L forms in solution were identical within error limits. Moreover, membrane binding of the differently labeled PEX5L was within detection limits identical, as obvious from the *z*-scan fluorescence profiles as shown in Figure 4A and B.

Optical and electrical recording from horizontal lipid bilayer

Single-molecule fluorescence methods as well as electrical single channel recordings have proven themselves as important methods in study of membrane proteins at a molecular level (Joo et al. 2008; Weatherill and Wallace 2015). Artificial lipid bilayers have already served for long time as a well-defined model system for high-resolution electrophysiological investigations of ion channel and large pore forming solute channels (porins) functions. Moreover, suitably designed microchips containing free-standing HLB allow the combination of electrophysiology with high-resolution nanoscopic fluorescence techniques thereby enabling the investigation of

the interaction of integral or membrane attached proteins. The HLB-technique has been shown to be a suitable technique to investigate the transition of soluble proteins to integral membrane proteins (Bartsch et al. 2012; Honigmann et al. 2010, 2012). The basic outlines and features of the combined opt-electrical recording using the HLB-technique is depicted in Figure 6. With the help of the FCS analysis of TCSPC data of fluorescence labeled proteins in solution and at/in membranes, information about their lateral diffusion and thus on their hydrodynamic properties can be obtained (Betaneli and Schwille 2013; Ries and Schwille 2012; Smith et al. 2017). The same applies to fluorescence anisotropy and FIDA analysis (Smith and Ghiggino 2015; Palo et al. 2002). Like FCS, the fluorescence intensity distribution analysis (FIDA) technique is based on the fluorescence fluctuation analysis by particularly monitoring heterogenous brightness profile and thus allowing to discriminate different fluorescent species according to their specific molecular brightness (Eggeling et al. 2003; Kask et al. 1999; Palo et al. 2002).

Electrical recording from artificial horizontal and vertical bilayer

The principle HLB setup used is shown in Figure 6 and the details and methods for analyzing the experimental data and the used instrumentation electrical single channel recording from artificial bilayer in combination with reconstituted proteins are given in large details elsewhere (Bartsch et al. 2013a, 2013b; Harsman et al. 2011). The vertical and the horizontal bilayer were composed of: 1,2-Dioleoyl-sn-Glycero-3-Phosphocholine (DOPC) and 1,2-Dioleoyl-sn-glycero-3-phosphoethanolamine (DOPE) (70/30). Buffer cis/trans: 250 mM KCl and 10 mM HEPES (4-(2-Hydroxyethyl)-1-piperazine ethane sulfonic acid) pH7.

MOCK-preparations from *E. coli* cells, which do not express PEX5Ls, were used as negative controls and showed no detectable ion channel activity. Also the truncated PEX5L(1–335) did not show any ion channel activity.

Furthermore, corresponding positive controls with OmpF (Ghai et al. 2018) and ColicinA (Honigmann et al. 2012) were carried out in the laboratory to calibrate the bilayer measuring stand, showing that the ion currents observed with Pex5L were characteristic of the PEX5L samples.

Hydrodynamic calculations

In order to relate the experimental obtained τ_{lat} and τ_{rot} values of the fluorescence labeled PEX5 in solution we can use known hydrodynamic relationships for a first reliable estimate of the hydrodynamic shape and size of PEX5 in solution. For this, we first assume that the PEX5 molecules have a spherical shape and that spherical oligomers with Ni(i = 1–8) can form from them. For FCS measurements, a calibration measurement is first made with a fluorophore (Atto655) whose diffusion coefficient is known to determine the focus size. The diffusion coefficient of PEX5 is calculated using the correlation time of PEX5 and the known focus size.

$$r_{focus} = \sqrt{4D_{Atto655} \cdot \tau_{Atto655}} \quad (1)$$

$$D_{pro} = \frac{r_{focus}^2}{4 \cdot \tau_{pro}} = \frac{k_B \cdot T}{f} = \frac{k_B \cdot T}{6 \cdot \pi \cdot \eta \cdot r_{pro}} \quad (2)$$

$$r_{pro} = \frac{k_B \cdot T}{6 \cdot \pi \cdot \eta} \cdot \frac{1}{D_{pro}} \quad (3)$$

$$V_{pro} = \frac{4}{3} \cdot \pi \cdot r_{pro}^2 ; \rho_{pro} = \frac{m_{pro}}{V_{pro}} ; mw_{pro} = mw_{hsPex5} = 7.0088\,\text{kDa} ; \rho_{pro} = 1.28 \frac{\text{g}}{\text{cm}^3} \quad (4)$$

$$mw_{pro}^{oligom} = mw_{hsPex5} \cdot i, \ (i = 1, 2 \ldots .8) \quad (5)$$

$$\tau_{FCS}^{oligom} = \frac{r_{focus}^2}{4 \cdot D_{FCS}^{oligom}} \quad (6)$$

$$\tau_{rot} = \frac{\eta \cdot V_{prot}}{k_B \cdot T} = \frac{1}{6 \cdot D_{rot}} ; \tau_{rot}^{oligom} = \frac{\eta \cdot V_{prot}^{oligom}}{k_B \cdot T} ; \eta = 0.96 \cdot 10^{-3}\,\text{Pa} \cdot \text{s} \quad (7)$$

Using equations (1)–(7) one can calculate τ_{FCS}^{oligom} and τ_{rot}^{oligom} as a function of the oligomeric state variable index (i). The results of this calculation are shown in Figure 3B and C.

Author contributions: All the authors have accepted responsibility for the entire content of this submitted manuscript and approved submission.

Research funding: This work was supported by the DFG research unit 'PerTrans' (FOR1905) to R.W and R.E. We would like to thank Prof. M. Winterhalter for support.

Conflict of interest statement: The authors declare no conflicts of interest regarding this article.

References

Alencastre, I.S., Rodrigues, T.A., Grou, C.P., Fransen, M., Sá-Miranda, C., and Azevedo, J.E. (2009). Mapping the cargo protein membrane translocation step into the PEX5 cycling pathway. J. Biol. Chem. 284: 27243–27251.

Bartsch, P., Harsman, A., and Wagner, R. (2013a). *Single channel analysis of membrane proteins in artificial bilayer membranes. Membrane Biogenesis*. Totowa, NJ, USA: Humana Press.

Bartsch, P., Harsman, A., and Wagner, R. (2013b). Single channel analysis of membrane proteins in artificial bilayer membranes. Membr. Biogen: Methods Protoc. 1033: 345–361.

Bartsch, P., Walter, C., Selenschik, P., Honigmann, A., and Wagner, R. (2012). Horizontal bilayer for electrical and optical recordings. Materials 5: 2705–2730.

Becker, W., Bergmann, A., Haustein, E., Petrasek, Z., Schwille, P., Biskup, C., Kelbauskas, L., Benndorf, K., Klocker, N., Anhut, T., et al. (2006). Fluorescence lifetime images and correlation spectra obtained by multidimensional time-correlated single photon counting. Microsc. Res. Tech. 69: 186–195.

Betaneli, V. and Schwille, P. (2013). Fluorescence correlation spectroscopy to examine protein-lipid interactions in membranes. Methods Mol. Biol. 974: 253–278.

Costa-Rodrigues, J., Carvalho, A.F., Fransen, M., Hambruch, E., Schliebs, W., Sá-Miranda, C., and Azevedo, J.E. (2005). Pex5p, the peroxisomal cycling receptor, is a monomeric non-globular protein. J. Biol. Chem. 280: 24404–24411.

Dal Peraro, M. and Van Der Goot, F.G. (2016). Pore-forming toxins: ancient, but never really out of fashion. Nat. Rev. Microbiol. 14: 77–92.

Eggeling, C., Gall, K., Palo, K., Kask, P., and Brand, L. (2003). Confocal fluorescence techniques in industrial application. In: *Proceedings of manipulation and analysis of biomolecules, cells, and tissues*, 4962. Biomedical Optics, San Jose, CA, US, p. 9.

Erdmann, R. and Schliebs, W. (2005). Peroxisomal matrix protein import: the transient pore model. Nat. Rev. Mol. Cell Biol. 6: 738–742.

Felekyan, S., Kühnemuth, R., Kudryavtsev, V., Sandhagen, C., Becker, W., and Seidel, C. (2005). Full correlation from picoseconds to seconds by time-resolved and time-correlated single photon detection. Rev. Sci. Instrum. 76: 083104.

Gaussmann, S., Gopalswamy, M., Eberhardt, M., Reuter, M., Zou, P., Schliebs, W., Erdmann, R., and Sattler, M. (2021). Membrane interactions of the peroxisomal proteins PEX5 and PEX14. Front. Cell Dev. Biol. 9: 1–14.

Ghai, I., Bajaj, H., Bafna, J.A., Hussein, H.A.E.D., Winterhalter, M., and Wagner, R. (2018). Ampicillin permeation across OmpF, the major outer-membrane channel in Escherichia coli. J. Biol. Chem. 293: 7030–7037.

Ghosh, M., Denkert, N., Reuter, M., Klümper, J., Reglinski, K., Peschel, R., Schliebs, W., Erdmann, R., and Meinecke, M. (2023). Dynamics of the translocation pore of the human peroxisomal protein import machinery. Biol. Chem. 404: 169–178.

Harsman, A., Bartsch, P., Hemmis, B., Kruger, V., and Wagner, R. (2011). Exploring protein import pores of cellular organelles at the single molecule level using the planar lipid bilayer technique. Eur. J. Cell Biol. 721–730, https://doi.org/10.1016/j.ejcb.2011.04.012.

Honigmann, A., Pulagam, L.P., Sippach, M., Bartsch, P., Steinhoff, H.-J., and Wagner, R. (2012). A high resolution electro-optical approach for investigating transition of soluble proteins to integral membrane proteins probed by colicin A. Biochem. Biophys. Res. Commun. 427: 385–391.

Honigmann, A., Walter, C., Erdmann, F., Eggeling, C., and Wagner, R. (2010). Characterization of horizontal lipid bilayers as a model system to study lipid phase separation. Biophys. J. 98: 2886–2894.

Jameson, D.M., Ross, J.A., and Albanesi, J.P. (2009). Fluorescence fluctuation spectroscopy: ushering in a new age of enlightenment for cellular dynamics. Biophys. Rev. 1: 105–118.

Joo, C., Balci, H., Ishitsuka, Y., Buranachai, C., and Ha, T. (2008). Advances in single-molecule fluorescence methods for molecular biology. Annu. Rev. Biochem. 77: 51–76.

Kask, P., Palo, K., Ullmann, D., and Gall, K. (1999). Fluorescence-intensity distribution analysis and its application in biomolecular detection technology. Proc. Natl. Acad. Sci. U. S. A. 96: 13756–13761.

Kerssen, D., Hambruch, E., Klaas, W., Platta, H.W., De Kruijff, B., Erdmann, R., Kunau, W.-H., and Schliebs, W. (2006). Membrane association of the cycling peroxisome import receptor Pex5p. J. Biol. Chem. 281: 27003–27015.

Kramar, P., Miklavčič, D., Kotulska, M., and Lebar, A.M. (2010). Chapter two - Voltage-and current-clamp methods for determination of planar lipid bilayer properties. In: *Advances in planar lipid bilayers and liposomes*, 11. Elsevier, pp. 26–69.

Meinecke, M., Bartsch, P., and Wagner, R. (2016). Peroxisomal protein import pores. Biochim. Biophys. Acta 1863: 821–827.

Meinecke, M., Cizmowski, C., Schliebs, W., Krüger, V., Beck, S., Wagner, R., and Erdmann, R. (2010). The peroxisomal importomer constitutes a large and highly dynamic pore. Nat. Cell Biol. 12: 273–277.

Miller, C. (2013). *Ion channel reconstitution*. Springer Science & Business Media.

Müller, C., Loman, A., Pacheco, V., Koberling, F., Willbold, D., Richtering, W., and Enderlein, J. (2008). Precise measurement of diffusion by multi-color dual-focus fluorescence correlation spectroscopy. Europhys. Lett. 83: 46001.

Palo, K., Brand, L., Eggeling, C., Jager, S., Kask, P., and Gall, K. (2002). Fluorescence intensity and lifetime distribution analysis: toward higher accuracy in fluorescence fluctuation spectroscopy. Biophys. J. 83: 605–618.

Patlak, J.B. (1993). Measuring kinetics of complex single ion channel data using mean-variance histograms. Biophys. J. 65: 29–42.

Prilipov, A., Phale, P.S., Van Gelder, P., Rosenbusch, J.P., and Koebnik, R. (1998). Coupling site-directed mutagenesis with high-level expression: large scale production of mutant porins from E. coli. FEMS Microbiol. Lett. 163: 65–72.

Ries, J. and Schwille, P. (2012). Fluorescence correlation spectroscopy. Bioessays 34: 361–368.

Rucktäschel, R., Girzalsky, W., and Erdmann, R. (2011). Protein import machineries of peroxisomes. Biochim. Biophys. Acta Biomembr. 1808: 892–900.

Sakmann, B. (2013). *Single-channel recording*. Springer Science & Business Media.

Salomons, F.A., Kiel, J.A., Faber, K.N., Veenhuis, M., and Van Der Klei, I.J. (2000). Overproduction of Pex5p stimulates import of alcohol oxidase and dihydroxyacetone synthase in a Hansenula polymorpha pex14Null mutant. J. Biol. Chem. 275: 12603–12611.

Shiozawa, K., Konarev, P.V., Neufeld, C., Wilmanns, M., and Svergun, D.I. (2009). Solution structure of human Pex5.Pex14.PTS1 protein complexes obtained by small angle X-ray scattering. J. Biol. Chem. 284: 25334–25342.

Skowyra, M.L. and Rapoport, T.A. (2022). PEX5 translocation into and out of peroxisomes drives matrix protein import. Mol. Cell 82: 3209–3225.e7.

Smith, D.A., Mckenzie, G., Jones, A.C., and Smith, T.A. (2017). Analysis of time-correlated single photon counting data: a comparative evaluation of deterministic and probabilistic approaches. Methods Appl. Fluoresc. 5: 042001.

Smith, T.A. and Ghiggino, K.P. (2015). A review of the analysis of complex time-resolved fluorescence anisotropy data. Methods Appl. Fluoresc. 3: 022001.

Wagner, R., Bhamidimarri, S.P., Brending, N., and Winterhalter, M. (2018). Electrophysiology on lipid bilayers combined with fluorescence imaging and spectroscopy. J. Phys. Appl. Phys. 51: 4.

Walter, T. and Erdmann, R. (2019). Current advances in protein import into peroxisomes. Protein J. 38: 351–362.

Weatherill, E.E. and Wallace, M.I. (2015). Combining single-molecule imaging and single-channel electrophysiology. J. Mol. Biol. 427: 146–157.